Estimates for the transverse single-spin asymmetries in $p^{\uparrow}p \to J/\psi X$ process at PHENIX RHIC and SPD NICA

A. V. Karpishkov[1,2], M. A. Nefedov[1], and V. A. Saleev[1,2]

[1] Samara National Research University, Samara, Russia
[2] Joint Institute for Nuclear Research, Dubna, Russia

24.03.2021
Quarkonia as Tools 2021

Outline

1. Generalized Parton Model (GPM) and it's application to calculation of TSSA
   - Factorization formula for the GPM
   - Polarized production. TSSA
   - Including ISI and FSI – Color Gauge Invariant formulation of GPM
2. TSSA in GPM and CGI-GPM
   - Numerical results. Comparison to PHENIX data
   - Numerical results. Predictions for NICA
3. Summary

Generalized Parton Model (GPM) and it's application to calculation of TSSA

Factorization schemes in different p_T-regions

The traditional Collinear Parton Model (CPM) is applicable in a region of high-p_T production

$$\mu \sim p_T \gg \Lambda_{QCD},$$

so we can neglect influence of small intrinsic $\mathbf{q_T}$ of initial partons ($\langle q_T^2 \rangle \simeq 1$ GeV^2).

But if we're interested in particle production in a region of $p_T \simeq \sqrt{\langle q_T^2 \rangle} \ll \mu$, we should take into account intrinsic q_T. It can be done within TMD approach, factorization for which has been proven in the limit $q_T \ll \mu$ [J. Collins, Camb. Monogr., Part. Phys. Nucl. Phys. Cosmol. 32, 1-624 (2011)]. In our case, the hard scale μ is given by charmonium mass $m_{\mathcal{C}} = 3.1 \div 3.7$ GeV.
So we can use phenomenological TMD-ansatz, a so called Generalized Parton Model (GPM), initial partons in which are on-shell:

$$q_\mu = xP_\mu^+ + yP_\mu^- + q_{T\mu}, (q_\mu)^2 = 0, \tag{1}$$

and a factorized prescription for TMD parton distribution functions (PDFs) is used:

$$F_a(x, q_T, \mu_F) = f_a(x, \mu_F) G_a(q_T), \tag{2}$$

where $f_a(x, \mu_F)$ – corresponding CPM PDF, $G_a(q_T)$ – Gaussian distribution $G_a(q_T) = \exp(-q_T^2 / \langle q_T^2 \rangle_a)/(\pi \langle q_T^2 \rangle_a)$.

Factorization formula for the GPM

Within the GPM we can write the following expression for the differential cross-section of $2 \to 1$ hard subprocess $g(q_1) + g(q_2) \to \mathcal{C}(k)$:

$$d\sigma(pp \to \mathcal{C}X) = \int dx_1 \int d^2\mathbf{q_{1T}} \int dx_2 \int d^2\mathbf{q_{2T}} \times \\ \times F_g(x_1, q_{1T}, \mu_F) F_g(x_2, q_{2T}, \mu_F) d\hat{\sigma}(gg \to \mathcal{C}), \quad (3)$$

where $\mathcal{C} = J/\psi, \psi(2S)$ or $\chi_c(1P)$, and

$$d\hat{\sigma}(gg \to \mathcal{C}) = (2\pi)^4 \delta^{(4)}(q_1 + q_2 - k) \frac{\overline{|M(gg \to \mathcal{C})|^2}}{2x_1 x_2 s} \frac{d^4k}{(2\pi)^3} \delta_+(k^2 - m_{\mathcal{C}}^2). \quad (4)$$

In a case of $2 \to 2$ subprocess $g(q_1) + g(q_2) \to \mathcal{C}(k) + g(q_3)$, $\mathcal{C} = J/\psi, \psi(2S)$ in formula (3) $d\hat{\sigma}(gg \to \mathcal{C})$ must be replaced by:

$$d\hat{\sigma}(gg \to \mathcal{C}g) = (2\pi)^4 \delta^{(4)}(q_1 + q_2 - k - q_3) \frac{\overline{|M(gg \to \mathcal{C}g)|^2}}{2x_1 x_2 s} \frac{d^3k}{(2\pi)^3 2k_0} \frac{d^4q_3}{(2\pi)^3} \delta_+(q_3^2). \quad (5)$$

Four-momenta of initial partons are on mass-shell ($q_1^2 = q_2^2 = 0$) and have longitudinal (along the Z-axis) and transverse parts:

$$q_1^\mu = \left(x_1 \frac{\sqrt{s}}{2} + \frac{\mathbf{q}_{1T}^2}{2\sqrt{s}x_1}, \mathbf{q}_{1T}, x_1 \frac{\sqrt{s}}{2} - \frac{\mathbf{q}_{1T}^2}{2\sqrt{s}x_1} \right)^\mu, \quad (6)$$

$$q_2^\mu = \left(x_2 \frac{\sqrt{s}}{2} + \frac{\mathbf{q}_{2T}^2}{2\sqrt{s}x_2}, \mathbf{q}_{2T}, -x_2 \frac{\sqrt{s}}{2} + \frac{\mathbf{q}_{2T}^2}{2\sqrt{s}x_2} \right)^\mu. \quad (7)$$

Single Spin Asymmetry

In inclusive process $p^{\uparrow}p \to \mathcal{C}X$ $\mathcal{C} = J/\psi, \chi_c, \psi(2S))$ TSSA is defined as:

$$A_N = \frac{d\sigma^{\uparrow} - d\sigma^{\downarrow}}{d\sigma^{\uparrow} + d\sigma^{\downarrow}} = \frac{d\Delta\sigma}{2d\sigma}. \tag{8}$$

The numerator and denominator of A_N have the form:

$$d\sigma \propto \int dx_1 \int d^2q_{1T} \int dx_2 \int d^2q_{2T} F_g(x_1, q_{1T}, \mu_F) F_g(x_2, q_{2T}, \mu_F) d\hat{\sigma}(gg \to \mathcal{C}X), \tag{9}$$

$$d\Delta\sigma \propto \int dx_1 \int d^2q_{1T} \int dx_2 \int d^2q_{2T} [\hat{F}_g^{\uparrow}(x_1, \mathbf{q}_{1T}, \mu_F) - \hat{F}_g^{\downarrow}(x_1, \mathbf{q}_{1T}, \mu_F)] \times F_g(x_2, q_{2T}, \mu_F) d\hat{\sigma}(gg \to \mathcal{C}X), \tag{10}$$

where $\hat{F}_g^{\uparrow,\downarrow}(x, q_T, \mu_F)$ is the distribution of unpolarized gluon (or quark) in polarized proton.
Following the Trento conventions [A. Bacchetta, U. DAlesio, M. Diehl and C. A. Miller, Phys. Rev. D **70**, 117504 (2004)], the gluon Sivers function (GSF) can be introduced as

$$\Delta\hat{F}_g^{\uparrow}(x_1, \mathbf{q}_{1T}, \mu_F) \equiv \hat{F}_g^{(\uparrow)}(x_1, \mathbf{q}_{1T}, \mu_F) - \hat{F}_g^{(\downarrow)}(x_1, \mathbf{q}_{1T}, \mu_F) = \\ = \Delta^N F_g^{\uparrow}(x_1, \mathbf{q}_{1T}^2, \mu_F) \cos(\phi_1) \equiv \left(-2\frac{q_{1T}}{M_p}\right) F_{1T}^{\perp g}(x_1, \mathbf{q}_{1T}^2, \mu_F) \cos(\phi_1). \tag{11}$$

Moreover, GSF must satisfy the positivity bound $\forall\ x_1, q_{1T}$:

$$\left|\Delta^N F_g^{\uparrow}(x_1, \mathbf{q}_{1T}^2, \mu_F)\right| \leq 2F_g(x_1, q_{1T}, \mu_F). \tag{12}$$

Single Spin Asymmetry within GPM and CGI-GPM frameworks

Figure 1 : Example diagrams for contributions to the numerator of TSSA in GPM (left panel) and CGI-GPM (right panel): ISI for production of ${}^3S_1^{(1)}$-state.

In GPM we can write the numerator of the asymmetry as follows:

$$d\Delta\sigma \propto \left(-2\frac{q_{1T}}{M_p}\right) F_{1T}^{\perp g}(x_1, \mathbf{q}_{1T}^2, \mu_F)\cos(\phi_1) \otimes F_g(x_2, q_{2T}, \mu_F) \otimes H^U_{gg\to cd}, \quad (13)$$

where $H^U_{gg\to cd} = \overline{|M(gg \to cd)|^2}$ – a coefficient-function in unpolarized case. Formally, the numerator of the asymmetry in the CGI-GPM approach ([L. Gamberg and Z. B. Kang, Phys. Lett. B **696**, 109 (2011)]) can be obtained from eq. (13) by with the substitution:

$$F_{1T}^{\perp g} H^U_{gg\to J/\psi g} \to \frac{C_I^{(f)} + C_{F_c}^{(f)}}{C_U} F_{1T}^{\perp g(f)} H^U_{gg\to J/\psi g} + \frac{C_I^{(d)} + C_{F_c}^{(d)}}{C_U} F_{1T}^{\perp g(d)} H^U_{gg\to J/\psi g} \equiv$$
$$\equiv F_{1T}^{\perp g(f)} H^{Inc(f)}_{gg\to J/\psi g} + F_{1T}^{\perp g(d)} H^{Inc(d)}_{gg\to J/\psi g}. \quad (14)$$

Feynman rules in the CGI-GPM and color factors for CSM

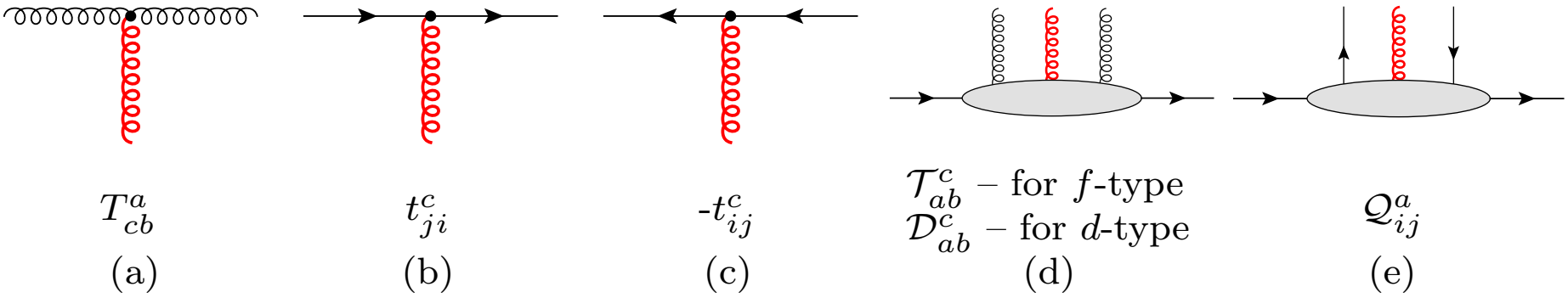

Figure 2 : Feynman rules for color factors within the CGI-GPM with additional eikonal gluon (with color index c).

The color factors are:

$$\mathcal{T}^c_{aa'} = \mathcal{N}_{\mathcal{T}} T^c_{aa'}, \mathcal{D}^c_{aa'} = \mathcal{N}_{\mathcal{D}} D^c_{aa'}, \mathcal{Q}^c_{ij} = \mathcal{N}_{\mathcal{Q}} t^c_{ij}, \tag{15}$$

where $T^a_{cb} \equiv -if_{acb}$, $D^a_{bc} \equiv d_{abc}$, $\mathcal{N}_{\mathcal{T}} = \frac{1}{Tr[T^c T^c]} = 1/(N_c(N_c^2-1))$, $\mathcal{N}_{\mathcal{D}} = \frac{1}{Tr[D^c D^c]} = 1/((N_c^2-4)(N_c^2-1))$, $\mathcal{N}_{\mathcal{Q}} = \frac{1}{Tr[t^c t^c]} = 2/(N_c^2-1)$.
So, correspondingly, for the f-type (C-even) and d-type (C-odd) GSF, the relative color factor is therefore calculated from Fig. 1 as follows:

$$\boxed{C_I^{(f)} = -\frac{1}{2} C_U, C_I^{(d)} = 0.} \tag{16}$$

And in CSM the color factor of the heavy quark-antiquark pair to the FSI:

$$\boxed{C_{F_c}^{(f)} = C_{F_c}^{(d)} = 0.} \tag{17}$$

Coefficient function for ICEM within the CGI-GPM

Figure 3 : Diagrams for contributions to the numerator of TSSA in CGI-GPM: FSI for $gg \to c\bar{c}$-process with both final-state quarks tagged.

In case of CGI-GPM factorization, the numerator of the TSSA has the form:

$$F_{1T}^{g(f)} \otimes \hat{\sigma}_{CGI}^{(f)}(\hat{s}, gg \to c\bar{c}) + F_{1T}^{g(d)} \otimes \hat{\sigma}_{CGI}^{(d)}(\hat{s}, gg \to c\bar{c}), \tag{18}$$

where $\hat{\sigma}_{CGI}^{(f/d)}(\hat{s}, gg \to c\bar{c})$ is the f/d-type coefficient function of CGI-GPM integrated over phase-space of final-state $c\bar{c}$-pair with fixed invariant mass $\hat{s}$. The f/d-type hard-scattering coefficients thus obtained have the form:

$$\begin{aligned}
H_{CGI}^{(f)}(gg \to c\bar{c}) &= \frac{8\pi^2\alpha_s^2}{N_c\left(N_c^2-1\right)\tilde{t}^2\tilde{u}^2}\left(4m_c^4(\tilde{t}+\tilde{u})^2 + 4m_c^2\tilde{t}\tilde{u}(\tilde{t}+\tilde{u}) - \tilde{t}\tilde{u}\left(\tilde{t}^2+\tilde{u}^2\right)\right), \\
H_{CGI}^{(d)}(gg \to c\bar{c}) &= N_c\frac{\tilde{t}-\tilde{u}}{\hat{s}}H_{CGI}^{(f)}(gg \to c\bar{c}), \\
H_{CGI}(q\bar{q} \to c\bar{c}) &= -H_{CGI}(\bar{q}q \to c\bar{c}) = \frac{8\pi^2\alpha_s^2(N_c^2+1)}{\hat{s}^2N_c^2}\left(2m_c^2\hat{s}+\tilde{t}^2+\tilde{u}^2\right),
\end{aligned}$$

where $\tilde{t} = \hat{t} - m_c^2$ and $\tilde{u} = \hat{u} - m_c^2$.

Cross sections for ICEM within the CGI-GPM

Figure 4 : Diagrams for contributions to the numerator of TSSA in CGI-GPM: FSI for $gg \to c\bar{c}$-process with both final-state quarks tagged.

Integrating this coefficient-functions over the phase-space of the final-state with fixed $c\bar{c}$ invariant-mass $\hat{s}$ one obtains:

$$\hat{\sigma}^{(f)}_{CGI}(\hat{s}, gg \to c\bar{c}) = \frac{\pi\alpha_S^2}{48\hat{s}}\left[(\frac{w^2}{2} - w - 1)\ln\left(\frac{1 - w/2 + \sqrt{1-w}}{1 - w/2 - \sqrt{1-w}}\right) + 2(1+w)\sqrt{1-w}\right], \quad (19)$$

$$\hat{\sigma}^{(d)}_{CGI}(\hat{s}, gg \to c\bar{c}) = 0, \quad (20)$$

$$\hat{\sigma}_{CGI}(\hat{s}, q\bar{q} \to c\bar{c}) = \frac{10\pi\alpha_S^2}{27\hat{s}}\left(1 + \frac{w}{2}\right)\sqrt{1-w}, \quad (21)$$

where $w = 4m_c^2/\hat{s}$.

TSSA in charmonium production at RHIC and NICA

PHENIX-2012 data, $|y| \leq 0.35$, $\sqrt{S} = 200$ GeV.

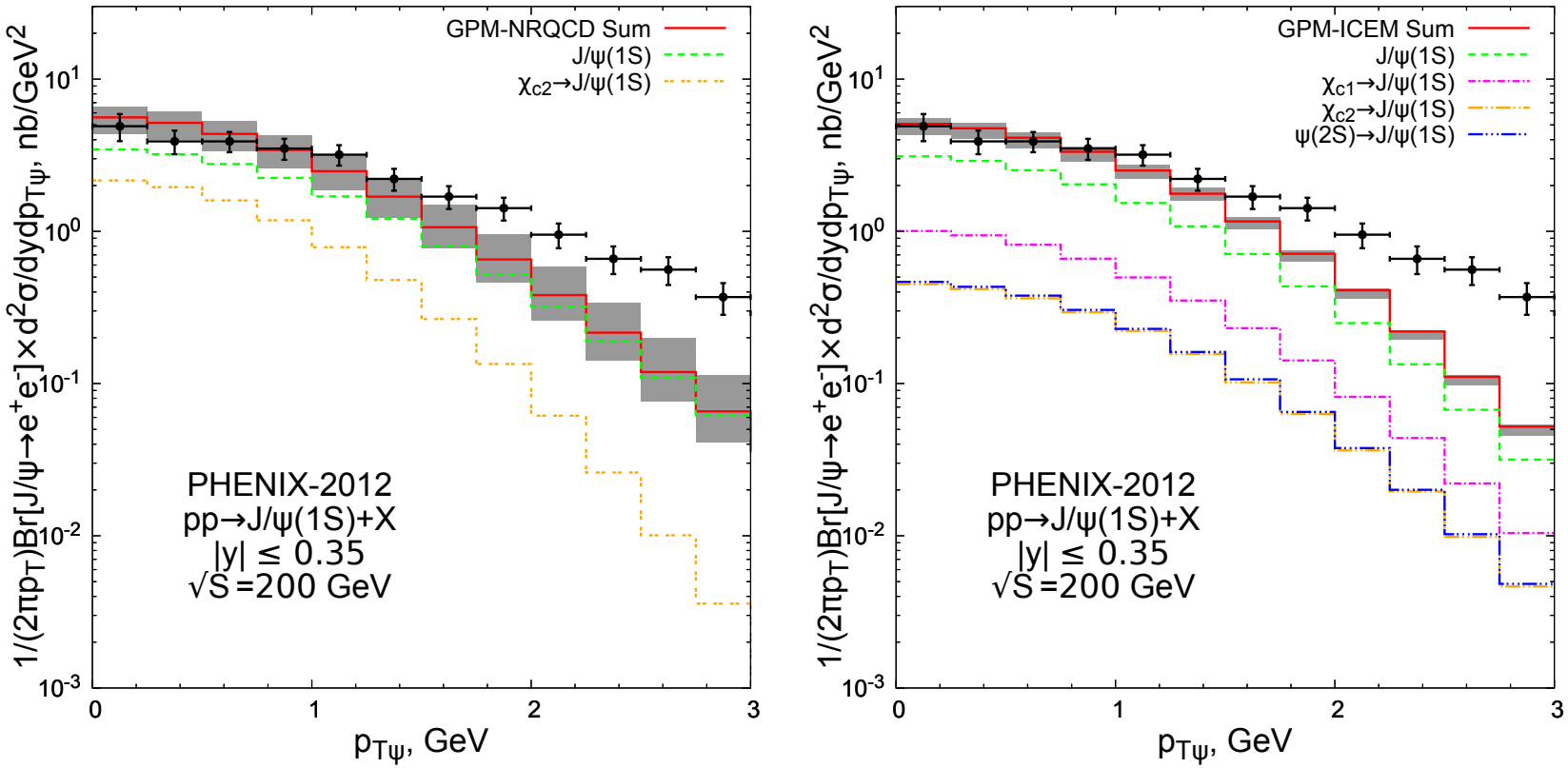

Figure 5 : Differential cross-section of prompt J/ψ production as function of transverse momentum at $\sqrt{s} = 200$ GeV, $|y| \leq 0.35$. The theoretical results are obtained in GPM with $\langle q_T^2 \rangle = 1$ GeV^2. Left panel: NRQCD-factorization prediction with only color-singlet channels included. Right panel: ICEM-prediction. In the left panel, non-zero contributions from decays $\chi_{c0} \to J/\psi$ and $\psi(2S) \to J/\psi$ are not shown. Experimental data are from the Ref. [A. Adare *et al.* [PHENIX], Phys. Rev. D **85**, 092004 (2012)].

PHENIX-2012 data, $|y| \leq 0.35$, $\sqrt{S} = 200$ GeV.

Table 1 : The relative contributions of direct and feed-down production within NRQCD and ICEM. Experimetal data of the PHENIX collaboration for $\sqrt{s} = 200$ GeV are from [A. Adare *et al.* [PHENIX], Phys. Rev. D **85**, 092004 (2012)].

$\sqrt{s}$	Model/Source of data	$\sigma^{\text{direct}} : \sigma^{\chi_c \to J/\psi} : \sigma^{\psi(2S) \to J/\psi}$
24 GeV	NRQCD	0.58 : 0.39 : 0.03
	ICEM	0.68 : 0.25 : 0.07
200 GeV	NRQCD	0.61 : 0.34 : 0.05
	ICEM	0.61 : 0.30 : 0.09
200 GeV	PHENIX collab.	0.58 : 0.32 : 0.10

Table 2 : The values of hadronization probabilities of ICEM, which had been obtained via the fit of total cross-section of J/ψ-production at PHENIX. The fit of LHC data are taken from [V. Cheung and R. Vogt, Phys. Rev. D **98**, 114029 (2018)].

$F_{\mathcal{C}}$	Our fit	The fit of LHC data
$F_{J/\psi}$	0.02	0.02
$F_{\chi_{c1}}$	0.06	0.18
$F_{\chi_{c2}}$	0.06	0.2
$F_{\psi'}$	0.08	0.12

PHENIX-2018 data, $1.2 \leq |y| \leq 2.2$, $\sqrt{S} = 200$ GeV.

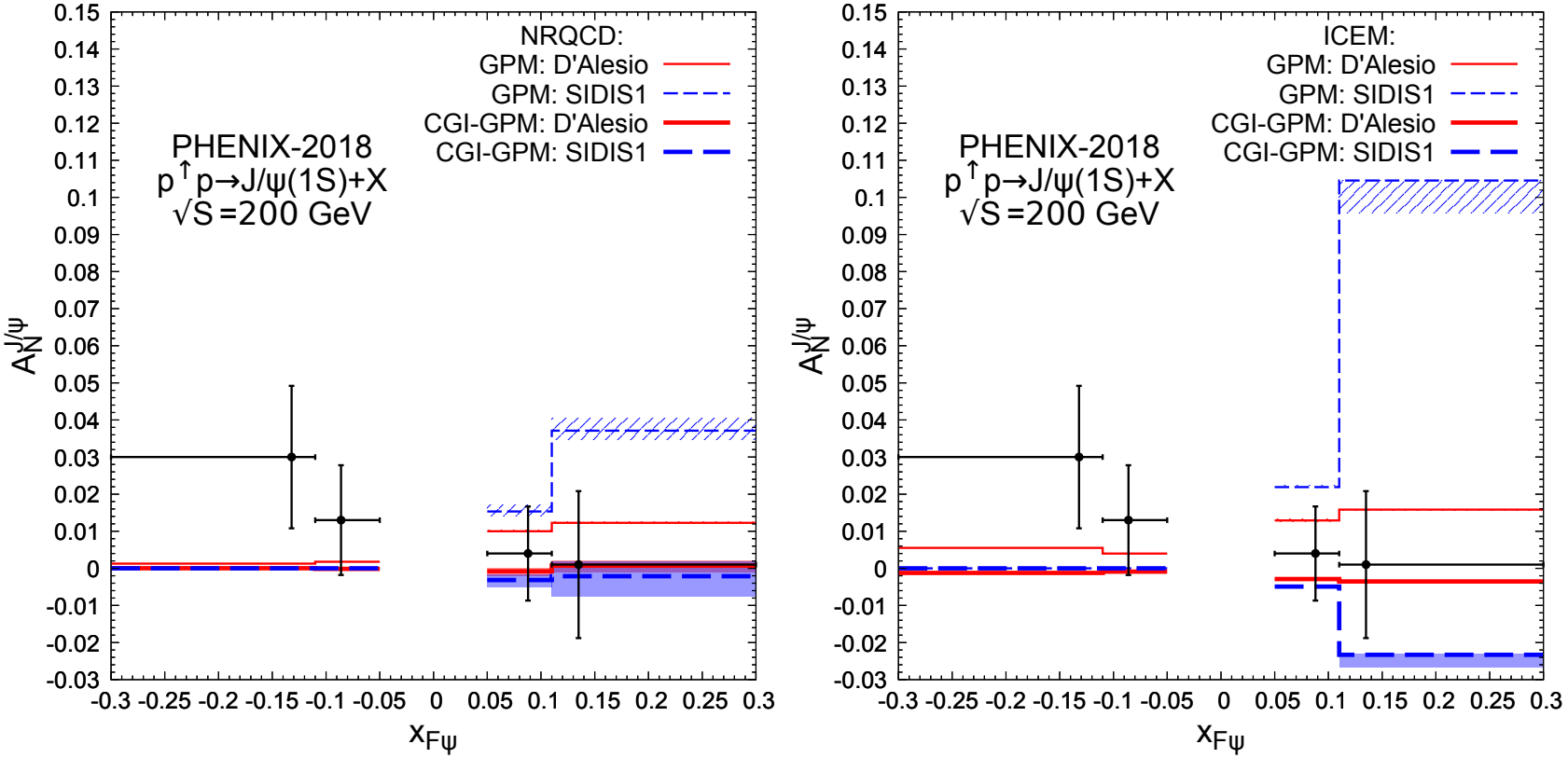

Figure 6 : TSSA $A_N^{J/\psi}$ as function of x_F at $\sqrt{s} = 200$ GeV within the GPM (thin histograms) and CGI-GPM (thick histograms). The theoretical results are obtained with SIDIS1 (dashed histograms) and D'Alesio *et al.* (solid histograms) parameterizations of GSFs. Left panel: NRQCD final-state factorization. Right panel: ICEM final-state factorization. Experimental data are from Ref. [C. Aidala *et al.* [PHENIX], Phys. Rev. D **98**, 012006 (2018)].

PHENIX-2018 data, $-2.2 \leq y \leq -1.2$, $\sqrt{S} = 200$ GeV.

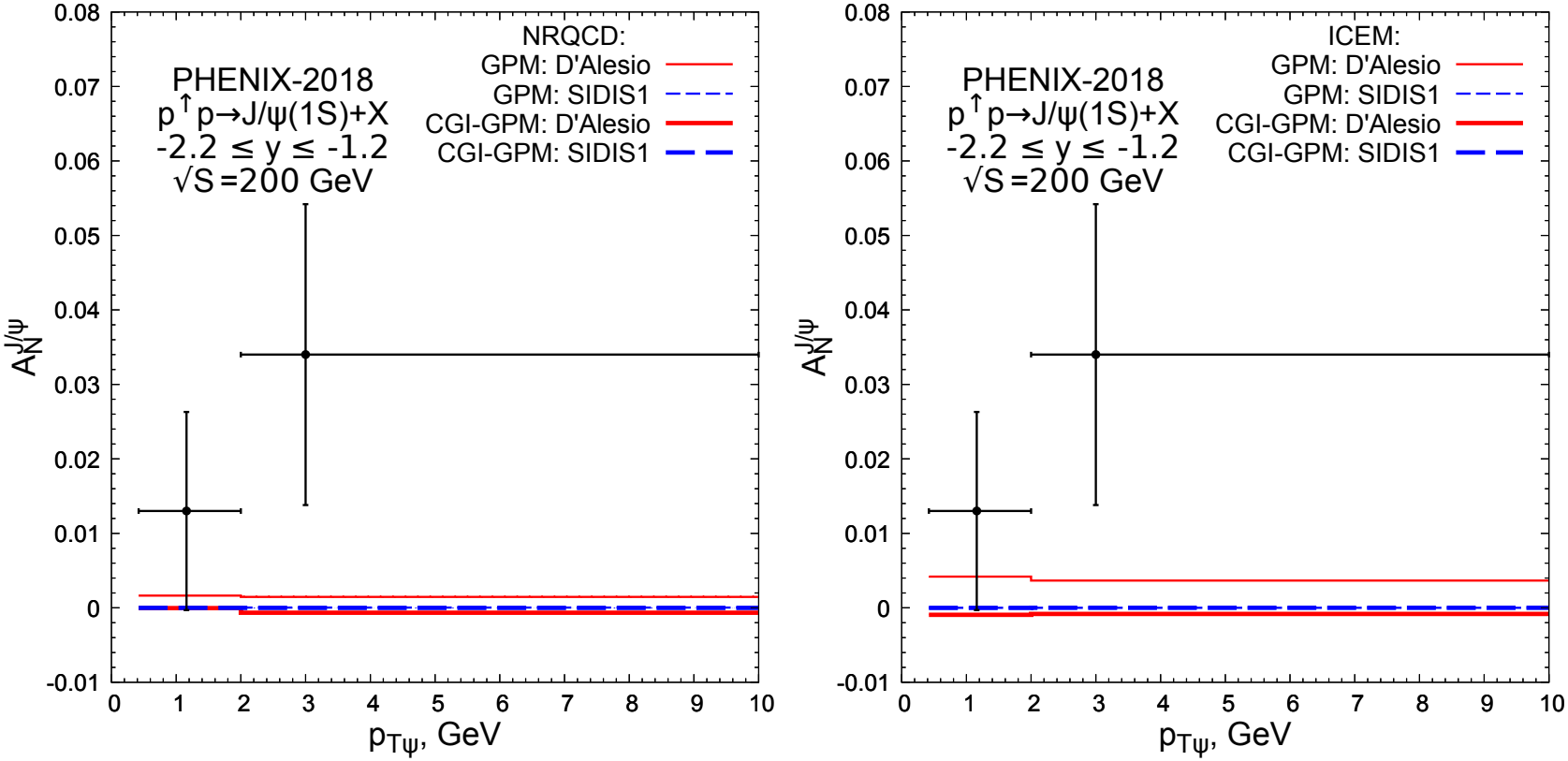

Figure 7 : TSSA $A_N^{J/\psi}$ as function of J/ψ-transverse momentum in backward region of rapidity at $\sqrt{s} = 200$ GeV within the GPM (thin histograms) and CGI-GPM (thick histograms). The theoretical results are obtained with SIDIS1 (dashed histograms) and D'Alesio *et al.* (solid histograms) parameterizations of GSFs. Left panel: NRQCD final-state factorization. Right panel: ICEM final-state factorization. Experimental data are from Ref. [C. Aidala *et al.* [PHENIX], Phys. Rev. D **98**, 012006 (2018)].

PHENIX-2018 data, $1.2 \leq y \leq 2.2$, $\sqrt{S} = 200$ GeV.

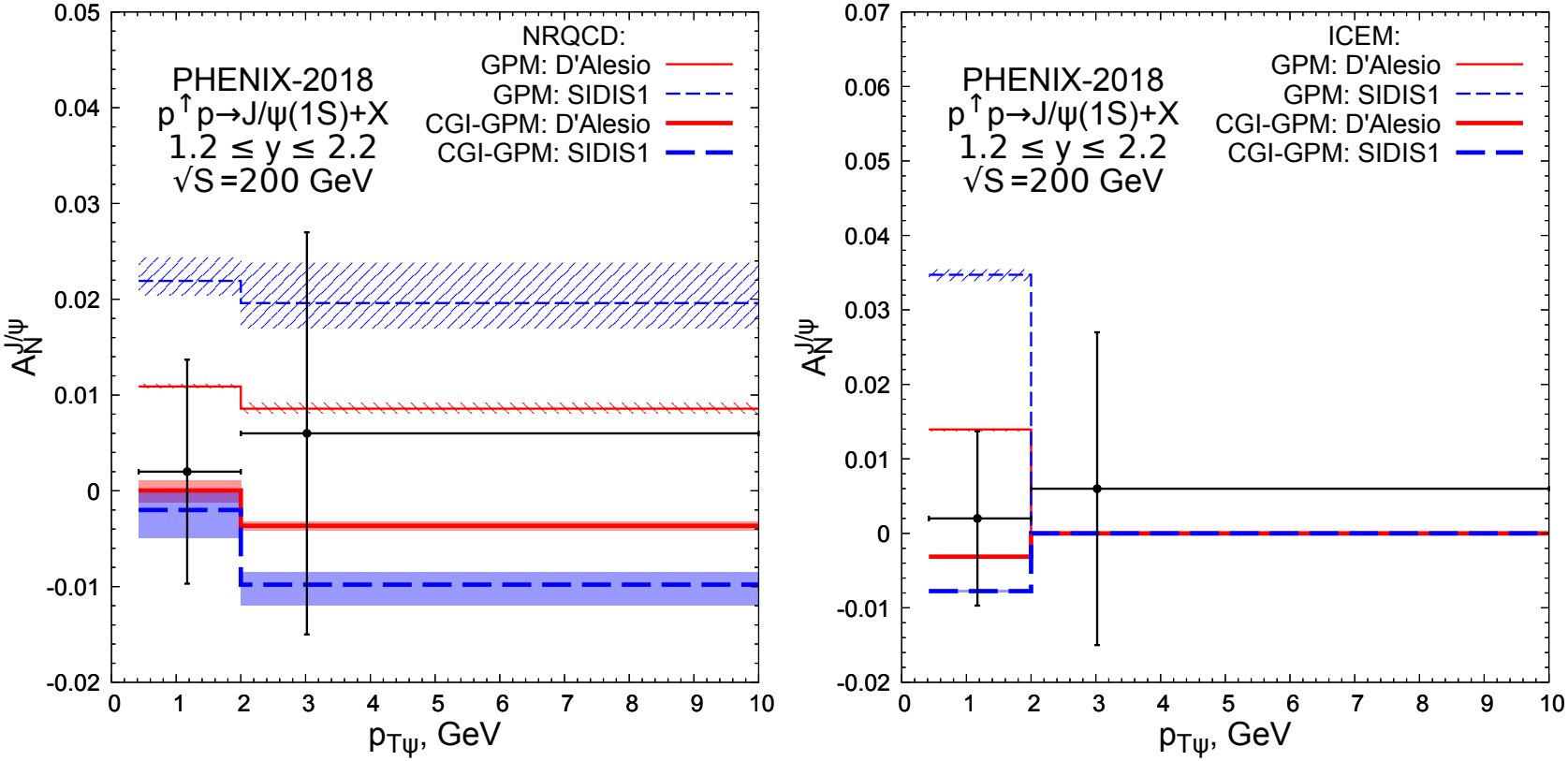

Figure 8 : TSSA $A_N^{J/\psi}$ as function of J/ψ-transverse momentum in forward region of rapidity at $\sqrt{s} = 200$ GeV within the GPM (thin histograms) and CGI-GPM (thick histograms). The theoretical results are obtained with SIDIS1 (dashed histograms) and D'Alesio *et al.* (solid histograms) parameterizations of GSFs. Left panel: NRQCD final-state factorization. Right panel: ICEM final-state factorization. Experimental data are from Ref. [C. Aidala *et al.* [PHENIX], Phys. Rev. D **98**, 012006 (2018)].

Predictions for NICA (in different models), $|y| \leq 3$, $\sqrt{S} = 24$ GeV.

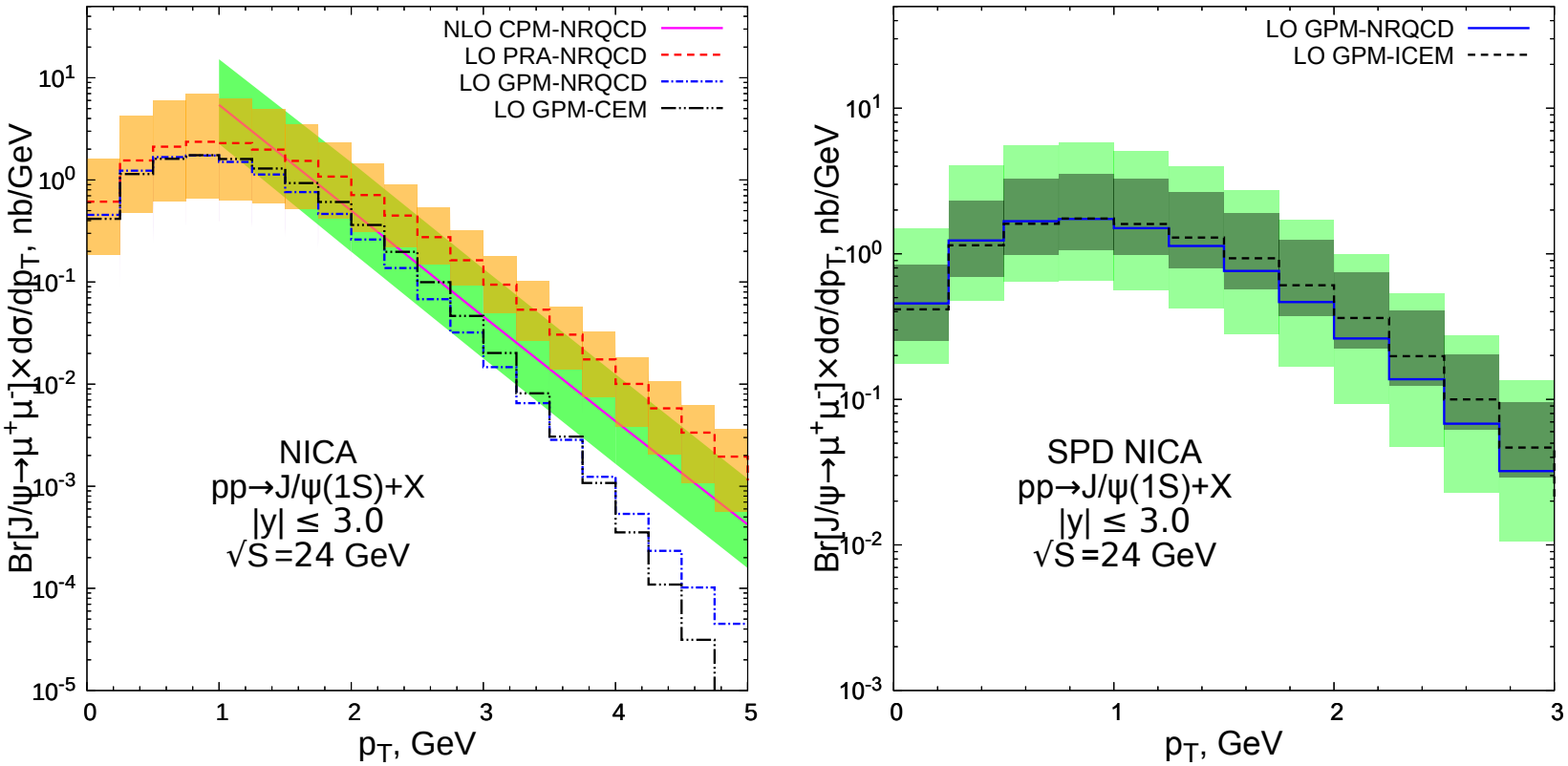

Figure 9 : Prompt J/ψ transverse momentum distribution at $\sqrt{s} = 24$ GeV, $|y| \leq 3$. Left panel: GPM results with $\langle q_T^2 \rangle = 1$ GeV^2 are shown by dash-dotted (NRQCD) and dash-double-dotted (ICEM) histograms. Solid and dashed histograms with uncertainty bands are PRA [A.V. Karpishkov, M.A. Nefedov and V.A. Saleev, J. Phys. Conf. Ser. **1435**, 012015 (2020)] and NLO CPM [M. Butenschön and B.A. Kniehl, private communication] predictions respectively. Right panel: GPM predictions in NRQCD (solid histogram with light green uncertainty band) and ICEM (dashed histogram with dark-green uncertainty band) approaches with their uncertainty bands shown.

Predictions for TSSA at NICA (D'Alesio), $|y| \leq 3$, $\sqrt{S} = 24$ GeV.

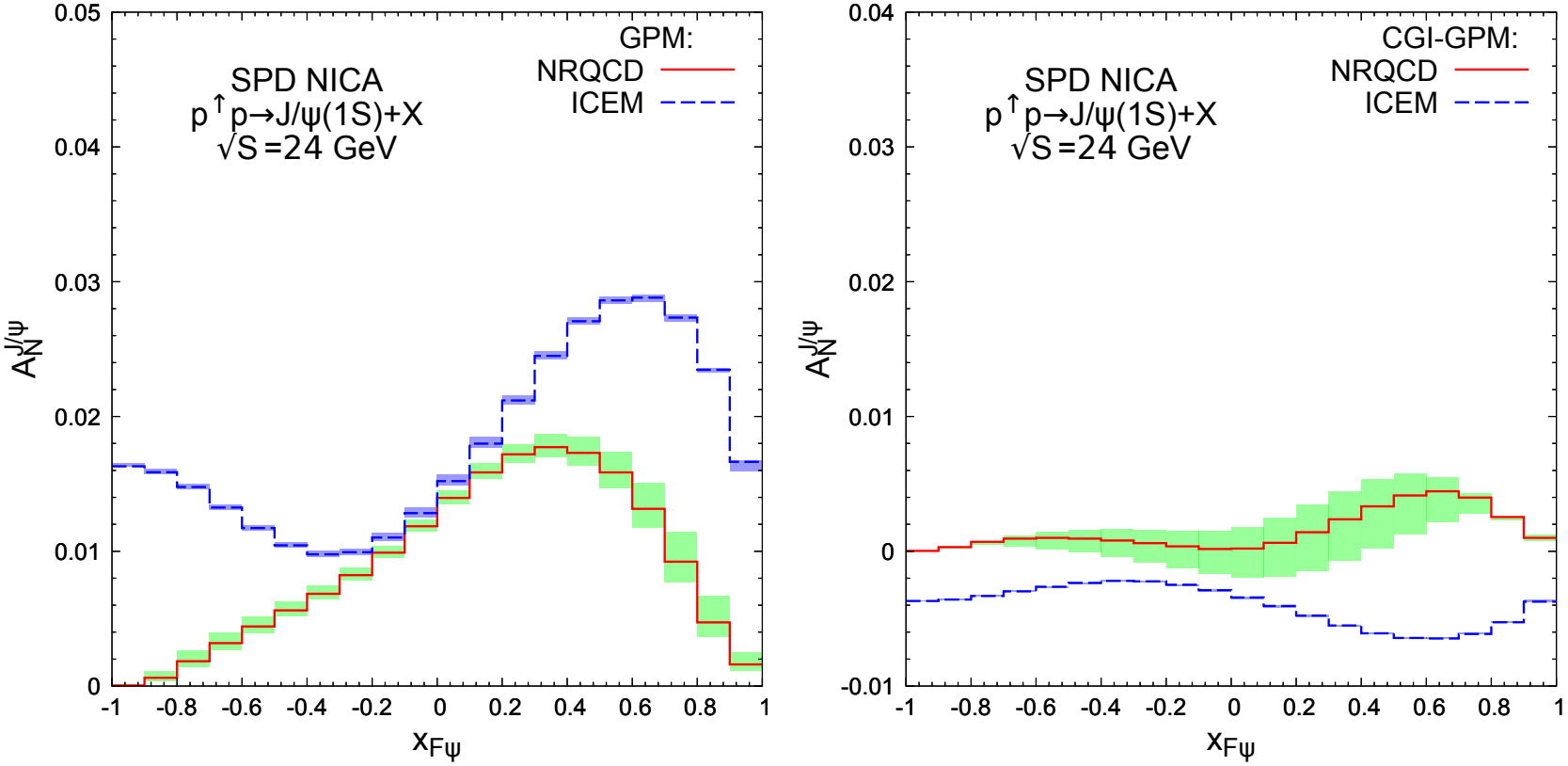

Figure 10 : Comparison of predictions for TSSA $A_N^{J/\psi}$ as function of x_F at $\sqrt{s} = 24$ GeV in NRQCD (solid histogram) and ICEM (dashed histogram) approaches. Left panel: GPM-prediction. Right panel: **CGI-**GPM-prediction. The D'Alesio *et al.* parametrisation of GSFs is used.

Predictions for TSSA at NICA (D'Alesio), $|y| \leq 3$, $\sqrt{S} = 24$ GeV.

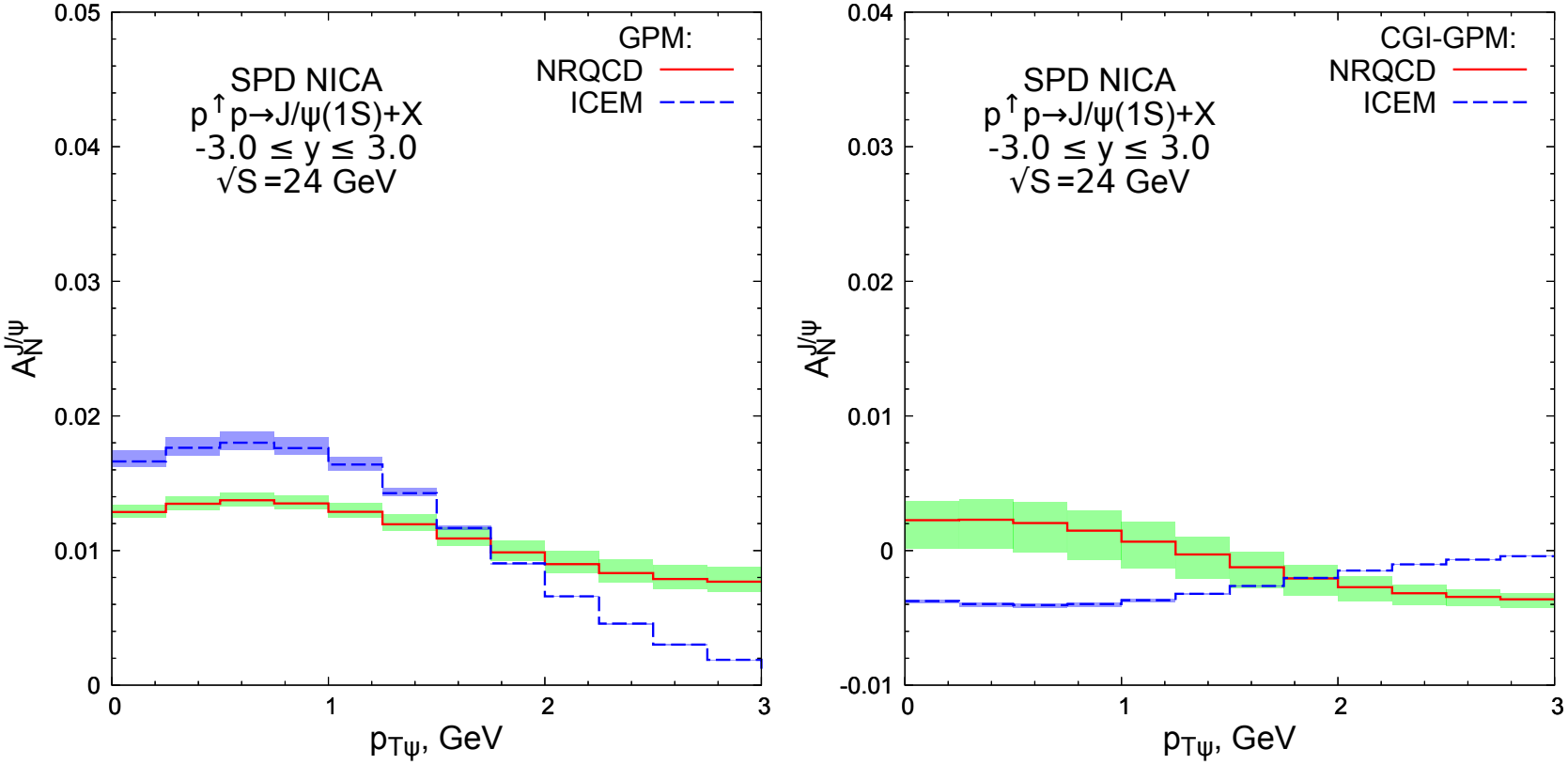

Figure 11 : Comparison of predictions for TSSA $A_N^{J/\psi}$ as function of p_T at $\sqrt{s} = 24$ GeV in NRQCD (solid histogram) and ICEM (dashed histogram) approaches. Left panel: GPM-prediction. Right panel: **CGI-**GPM-prediction. The D'Alesio *et al.* parametrisation of GSFs is used.

Predictions for TSSA at NICA (SIDIS1), $|y| \leq 3$, $\sqrt{S} = 24$ GeV.

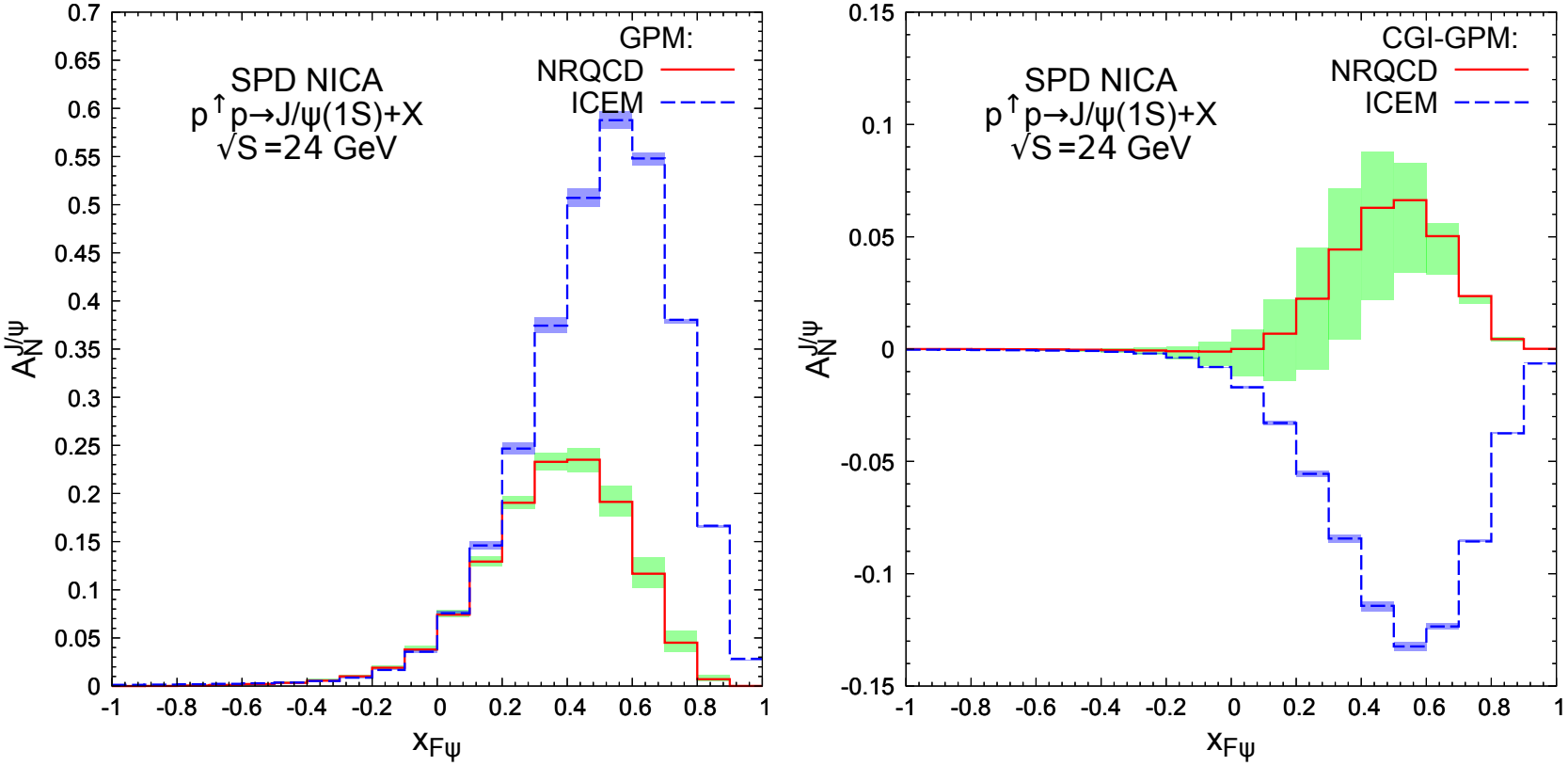

Figure 12 : Comparison of predictions for TSSA $A_N^{J/\psi}$ as function of x_F at $\sqrt{s} = 24$ GeV in NRQCD (solid histogram) and ICEM (dashed histogram) approaches. Left panel: GPM-prediction. Right panel: **CGI-**GPM-prediction. The SIDIS1 parametrisation of GSFs is used.

Predictions for TSSA at NICA (SIDIS1), $|y| \leq 3$, $\sqrt{S} = 24$ GeV.

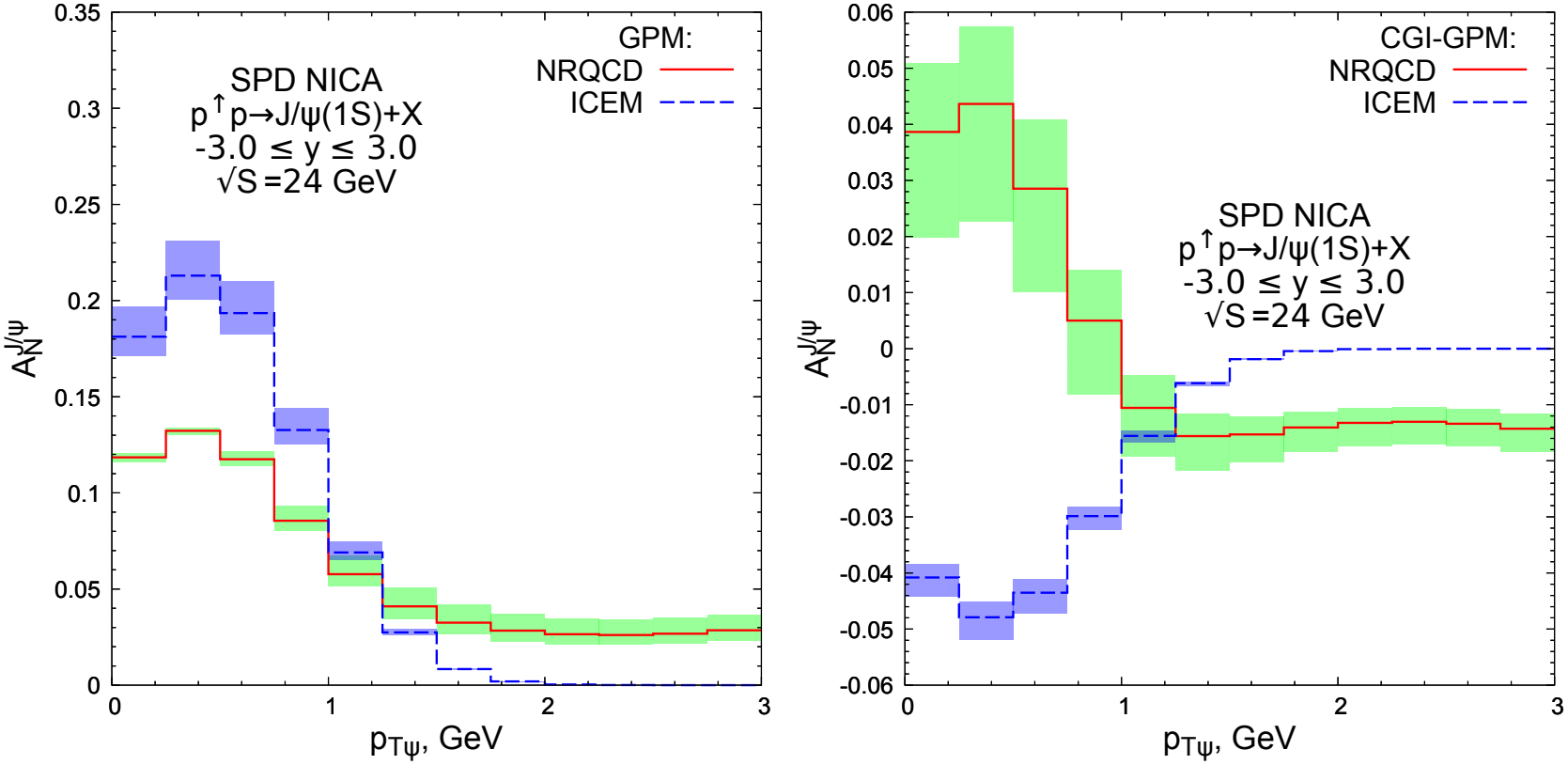

Figure 13 : Comparison of predictions for TSSA $A_N^{J/\psi}$ as function of p_T at $\sqrt{s} = 24$ GeV in NRQCD (solid histogram) and ICEM (dashed histogram) approaches. Left panel: GPM-prediction. Right panel: **CGI-**GPM-prediction. The SIDIS1 parametrisation of GSFs is used.

Summary

- We have found that taking into account only color-singlet production mechanism, the good description of prompt J/ψ transverse momentum spectra at small $k_{T\,J/\psi} < m_{J/\psi}$ can be achieved in GPM. Our NRQCD calculation leads to total cross-section ratios of direct and feed-down contributions in good agreement with experimental data.
- The Color Gauge Invariant formulation of the GPM is able to reproduce the expected opposite relative sign of the Sivers asymmetries, due to the effects of FSIs and ISIs.
- We also see sizeable differences between NRQCD and ICEM predictions of charmonium TSSA within both GPM and CGI-GPM.
- In CGI-GPM within both the frameworks of CSM and ICEM the process $p^{\uparrow}p \to \mathcal{H}X$ of *direct production* of $J/\psi(\psi')$ is sensitive to f-type GSF. While the χ_c production within the CSM is sensitive to d-type GSF and to f-type within the ICEM.

Thank you for your attention!

Backup: an estimation of quark contribution to the TSSA at PHENIX within ICEM

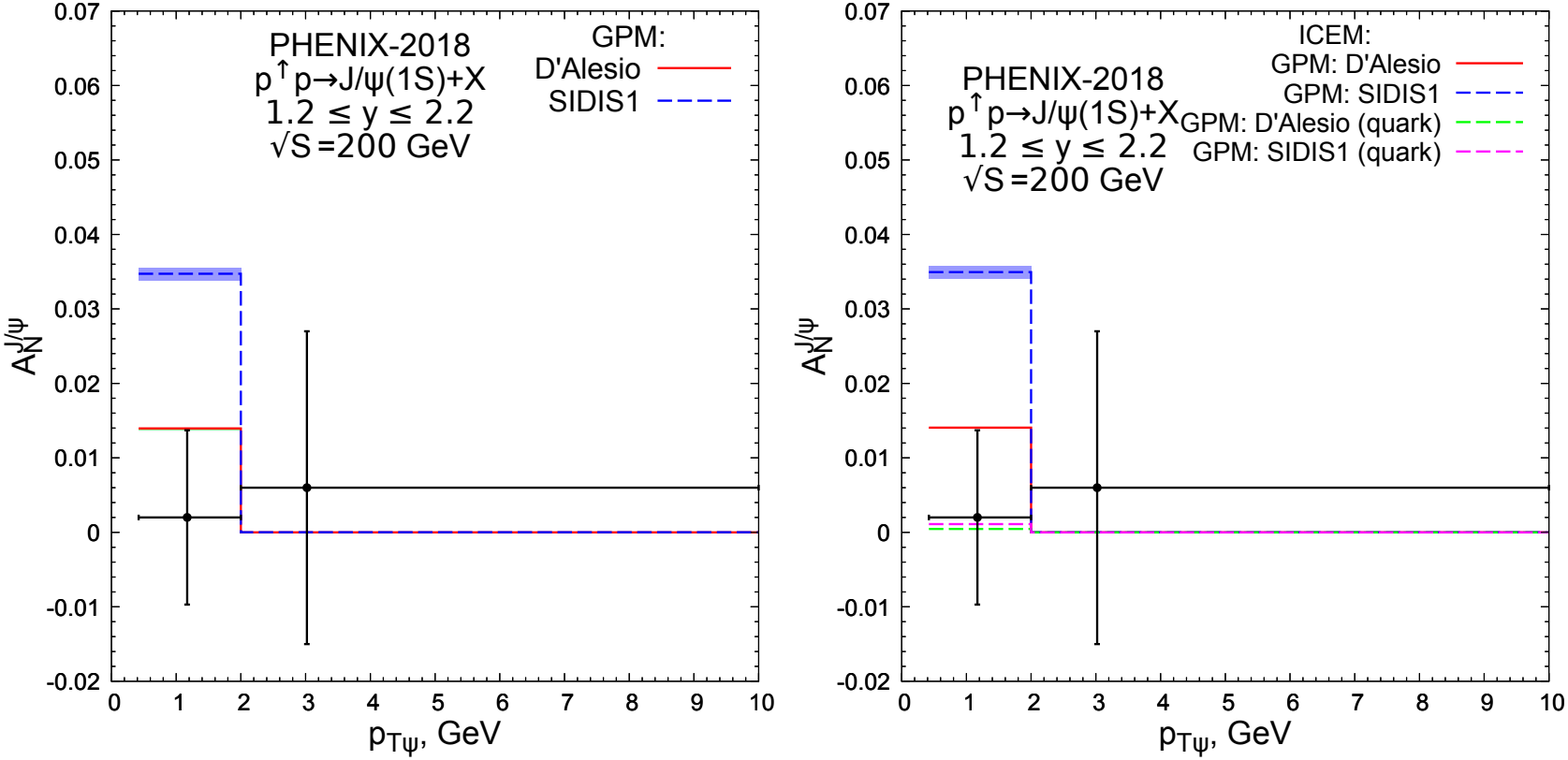

Figure 14 : TSSA $A_N^{J/\psi}$ as function of J/ψ-transverse momentum in forward region of rapidity at $\sqrt{s} = 200$ GeV within the GPM without (left panel) and with (right panel) quark contribution. The theoretical results are obtained with SIDIS1 and D'Alesio *et al.* parameterization of GSFs and ICEM final-state factorization. Experimental data are from Ref. [C. Aidala *et al.* [PHENIX], Phys. Rev. D **98**, 012006 (2018)].

Backup: an estimation of quark contribution to the TSSA at PHENIX within ICEM

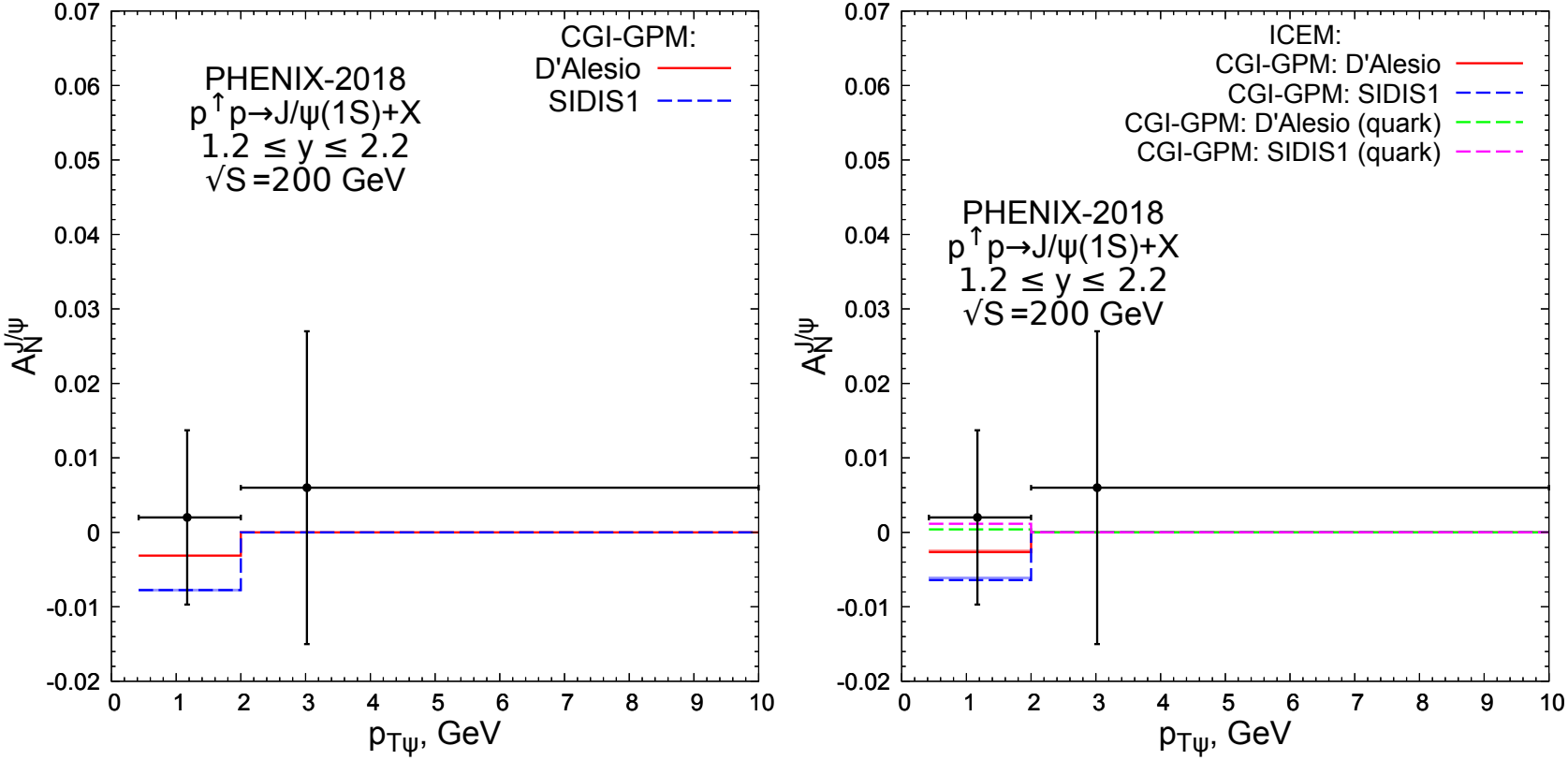

Figure 15 : TSSA $A_N^{J/\psi}$ as function of J/ψ-transverse momentum in forward region of rapidity at $\sqrt{s} = 200$ GeV within the CGI-GPM without (left panel) and with (right panel) quark contribution. The theoretical results are obtained with SIDIS1 and D'Alesio *et al.* parameterization of GSFs and ICEM final-state factorization. Experimental data are from Ref. [C. Aidala *et al.* [PHENIX], Phys. Rev. D **98**, 012006 (2018)].

Backup: an estimation of quark contribution to the TSSA at SPD within ICEM

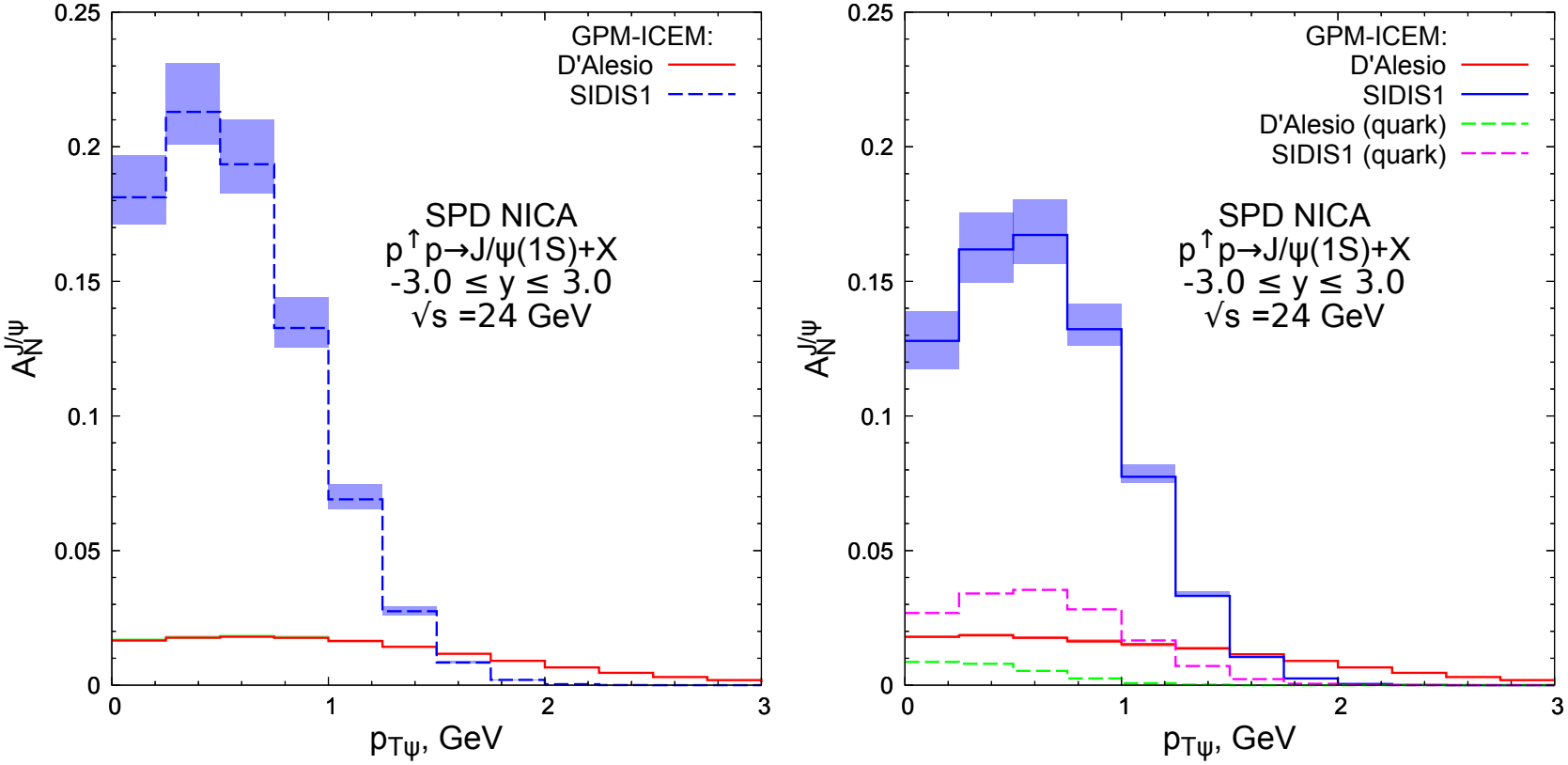

Figure 16 : Comparison of predictions for TSSA $A_N^{J/\psi}$ as function of J/ψ-transverse momentum at $\sqrt{s} = 24$ GeV within the GPM without (left panel) and with (right panel) quark contribution. The theoretical results are obtained with SIDIS1 and D'Alesio *et al.* parameterization of GSFs and ICEM final-state factorization.